Research Article

Chu Cheng*, Yan-Shuo Feng, Ming-Yu Li, Meng-Xin Wang, Tao Huang, Ling-Ling Xiong, and Xiao-Heng Li

Design and preparation of micro-nano dual-scale particle-reinforced Cu–Al–V alloy: Research on the aluminothermic reduction process

https://doi.org/10.1515/ntrev-2025-0213
received June 1, 2025; accepted August 26, 2025

Abstract: In this study, an innovative idea of preparing dual-phase micro-nano particle reinforced copper-based materials by one-step aluminothermic reduction method is proposed. That is, copper-based materials containing uniformly distributed dual-phase micro-nano particle reinforced phases were obtained by aluminothermic reduction reaction directly using aluminum powder, vanadium oxide, copper oxide, *etc.*, as raw materials. A systematic investigation was conducted on the thermodynamic behavior of the reaction system for dual-phase micro-nano particle-reinforced copper matrix composites, accompanied by comprehensive characterization of the resultant metallic alloys and slag phases. The results show that the dual-phase micro-nano particle composite reinforced copper-based materials were successfully prepared by aluminothermic reduction method. There are 1–10 μm micron vanadium particles and 60–200 nm nano-vanadium-aluminum master alloy phases dispersed in the microstructure of copper-based materials. With the increase in V_2O_5 ratio, the size of micron vanadium particles in the prepared dual-phase micro-nano particle reinforced copper-based material gradually increases, and the size of Al_xV_y phase dispersed in the matrix gradually decreases. The inclusions in the copper matrix are mainly Al_2O_3, and the reducing slag is mainly composed of $CaAl_4O_7$, $CaAl_2O_4$, and Cu_2O.

Keywords: copper alloys melt, aluminothermic reduction, *in situ* synthesis, micro-nano particles

1 Introduction

Due to their exceptional electrical conductivity and mechanical strength, copper-based composites have become critical materials in advanced engineering applications, serving as key components in electrical connectors, high-speed rail contact wires, and integrated circuit lead frames [1,2]. With the rapid development of the power, electronics, and electromagnetic fields, higher requirements have been put forward for the comprehensive properties of copper-based materials, such as high-temperature mechanical properties, wear resistance, and electrical properties [3]. Particle strengthening refers to a strengthening method that introduces second-phase particles with high strength, high modulus, and certain size as reinforcing materials into the metal matrix, thereby improving the performance of metal matrix composites [4–6]. However, when the size of the second phase particles is small (d = 0.01–0.1 μm), it belongs to dispersion strengthening, and its strengthening mechanism is Orowan mechanism, which can significantly improve the strength of metal matrix composites. When the second phase particle size is large (d = 1.0–50 μm), it belongs to particle strengthening, and its strengthening mechanism is Ansel-Lenier mechanism, which can significantly improve the wear resistance of the material [7]. Zhu *et al.* fabricated a multiscale layered (Ti_x, Nb_{1-x}) surface enhancement layer on a high-temperature Ti–Nb alloy substrate *via* the *in situ* solid-state diffusion method. This surface modification yielded a Ti–Nb alloy exhibiting significantly enhanced strength and wear resistance [8]. This demonstrates that the incorporation of micro-nano dual-phase particles within the alloy matrix significantly enhances both strength and wear resistance.

*** Corresponding author: Chu Cheng,** School of Materials Science and Engineering, Henan University of Science and Technology, Luoyang, 471023, China; Henan Key Laboratory of Non-ferrous Materials Science & Processing Technology, Henan University of Science and Technology, Luoyang, 471003, China; State Key Laboratory of Light Superalloys, Luoyang, 471023, China, e-mail: cheng_chu_love@126.com
Yan-Shuo Feng, Ming-Yu Li, Meng-Xin Wang, Tao Huang: School of Materials Science and Engineering, Henan University of Science and Technology, Luoyang, 471023, China
Ling-Ling Xiong: Sanmenxia Nonferrous Metals Technology Development Center, Sanmenxia, 4472100, China
Xiao-Heng Li: Henan Zhongyuan Gold Smelter., LLC, Sanmenxia, 472100, China

At present, the methods of introducing particle reinforced phase into copper matrix mainly include direct addition method and *in situ* synthesis method. The direct addition method is to directly add the second phase particles directly into the copper melt during the preparation of the copper-based material and stir evenly or uniformly mix the second phase particles with the copper powder before sintering. The former is called stirring addition method, and the latter is called powder metallurgy method. Copper matrix composites with excellent mechanical properties can be prepared by adding ceramic particles and other strengthening phases into copper by stirring addition method [9,10]. The stirring addition method has the advantages of simple operation, low cost, and high production efficiency. However, the stirring addition method has the disadvantages of poor interface bonding and uneven dispersion between the second phase particles and the copper matrix [11,12]. The problem of poor interfacial bonding between the second phase particles and the copper matrix was solved by using copper plating pretreatment of the second phase particles and adding carbide forming elements to the copper matrix [13,14]. By using ultrasonic dispersion, electromagnetic stirring, and other methods, the dispersion uniformity of particles in copper matrix is improved and the problem of uneven dispersion is solved [15,16].

Through the powder metallurgy method, the particle reinforced phase added to copper can be more uniform, so as to effectively improve the mechanical properties of copper matrix composite materials. Liu *et al.* developed wear-resistant and corrosion-resistant copper matrix composites by adding nano-Bi powder, SiC or ceramic hybrid composites, carbon nanotubes (CNT), and alumina nanoparticles to copper [17–19]. The *in situ* synthesis method is to directly synthesize the fine particle reinforced phase in the metal matrix, which has the characteristics of good bonding between the reinforced phase and the matrix interface and uniform dispersion. Shen *et al.* [20] prepared Cu–Cr alloy with Cr content of 0.47–4.92 wt%, high strength, high conductivity, and excellent tensile strength by the reduction reaction of Cr_2O_3 and Cu–Mg melt and heat treatment. Zhang *et al.* [21] adjusted the amount of Zr and B to make the *in situ* reaction between Zr and B in the copper melt to form micron-sized ZrB_2 particles with contents of 0, 1.0, and 1.5 wt%, respectively. After aging treatment, nano-sized Cu_5Zr precipitates were formed to obtain copper-based composites with good mechanical properties and electrical conductivity. The powder metallurgy method directly mixes the raw materials of the synthesized target particles during the mixing process, and prepares the alloy with TiC and TiB_2 particle phases by *in situ* synthesis [22,23].

The aluminothermic reduction method is widely used in the preparation of high melting point ferroalloys such as ferromolybdenum, ferrotungsten, and ferrotitanium. Due to the presence of oxide inclusions, ferroalloys can only be used as additives or deoxidizers for steelmaking, but not as structural and functional materials [24–26]. Dou and Cheng *et al.* used aluminothermic reduction to obtain a high-temperature metal and slag mixed melt, and then combined with modern metallurgical technologies such as electromagnetic coupling refining and vacuum self-consuming refining to successfully prepare CuCr25~40 and CuW50 contact materials [27,28]. The size of *in situ* synthesized tungsten particles in the prepared tungsten-copper composites is 0.82–2.03 μm. Dou *et al.* [29] combined magnesiothermic reduction with modern hydrometallurgy to prepare ultrafine W, Mo, Ti, and other high melting point metal powders. Nersisyan *et al.* [30] prepared spherical tungsten powder with particle size of 20–50 nm by molten salt assisted-magnesium thermal self-propagating high-temperature synthesis. Therefore, aluminothermic reduction has certain advantages in the preparation of ultrafine metal powder and copper-based materials containing ultrafine particles.

According to the design principle of metal matrix composites, a copper matrix composite containing micron-sized vanadium particles and nano-sized vanadium-aluminum intermediate compound particles was designed to develop a new type of high-strength and high-wear copper matrix material. Furthermore, a novel synthesis method utilizing aluminothermic reduction followed by refining under heat preservation was proposed for the preparation of this copper-based material. The flow chart is shown in Figure 1.

Using CuO and V_2O_5 as raw materials, Al as reducing agent, and CaO as slagging agent, the high temperature gold-slag mixed melt was obtained by aluminothermic reduction. After preliminary slag-metal separation, the Cu–Al–V alloy melt containing micron V particles and nano-Al_xV_y was obtained. Then, the refining slag was added for refining under heat preservation to further remove the oxide inclusions, and the micro-nano dual-scale Cu–Al–V alloy ingot was obtained after casting cooling. In this study, the process of preparing Cu–Al–V melt containing different contents of micron vanadium particles and nano-vanadium-aluminum intermediate compounds by aluminothermic reduction was studied. Thermodynamic calculations were performed on the reaction system, followed by systematic characterization and analysis of the resulting Cu–Al–V melt composition and slag phase. This study provides a basis for the composition control of copper matrix composites containing different contents of micron vanadium particles and nano-vanadium-aluminum intermediate compounds, which is of great significance for the development of high-strength and high-wear-resistant copper alloys and their preparation technology.

2 Materials and experimental procedure

2.1 Materials

Vanadium pentoxide (99 wt% V_2O_5, particle size: 80–100 nm) and copper oxide (99.50 wt% CuO, particle size: 30–38 μm) were used as raw materials. Aluminum particle (99.5% pure, particle diameter: 0.1–3 mm) was used as a reductant. CaO (99% pure, particle diameter: ≤0.25 mm) and magnesium powder (99.5% pure, particle diameter: ≤0.2 mm) were supplied by Sinopharm Chemical Reagent Co., Ltd, China.

2.2 Experimental methods

First, the materials of copper oxide, vanadium pentoxide, and calcium oxide required for the experiment were put into the oven, dried for 12 h at 523 K, and then mixed for 1 h on the ball mill mixer. After the mixing, it was preheated at 353 K for 30 min. Finally, the preheated material is accumulated at the bottom of the graphite crucible, and the magnesium powder is used as the ignition agent to induce the self-propagating high-temperature synthesis (SHS) reaction. After natural cooling, the alloy ingot and slag are obtained. The mass ratios of CuO, V_2O_5, and Al particles in the three groups of experiments were 1:0.075:0.26, 1:0.25:0.35, and 1:0.36:0.40, respectively. The ratios of CaO in the ingredients can be expressed as $R_{(C/A)}$ (the molar ratio of CaO to Al_2O_3, and Al_2O_3 is a combustion product of the SHS reaction in theoretical stoichiometry). The $R_{(C/A)}$ in the experiments was 1.25.

2.3 Analysis methods

The microstructure of the alloy was observed by an inverted metallographic microscope (Axio Vert A1, Zeiss, Germany). Cu–Al–V composites were characterized by scanning electron microscopy (SEM, JSM-7800F, Hitachi, Japan). X-ray fluorescence spectrometer (XRF; Thermo Scientific ARL 4460, Germany) was used for accurate determination of chemical composition in alloys. The nanoparticles in the alloy were characterized by transmission electron microscopy (TEM, JEM-2100, JEOL, Japan). The slag obtained by aluminothermic reduction was characterized by X-ray diffractometer (Model D8 Bruker, Germany). The Cu *k*-*α*1 source was 40 kV, 40 mA.

In order to further analyze the size and morphology of inclusions in copper-aluminum-vanadium composites, the inclusions in copper-aluminum-vanadium composites with V content of 5, 15, and 20% were extracted. The tungsten-copper composite sample was placed in a mixed solution of $FeCl_3$ and dilute hydrochloric acid to completely dissolve the copper matrix in the sample, and then ultrasonically cleaned with pure water. Finally, the inclusion particles were obtained by vacuum drying. Then, the morphology and phase of the extracted inclusions were characterized by SEM, and the particle size of the extracted inclusions was counted by ImageJ.

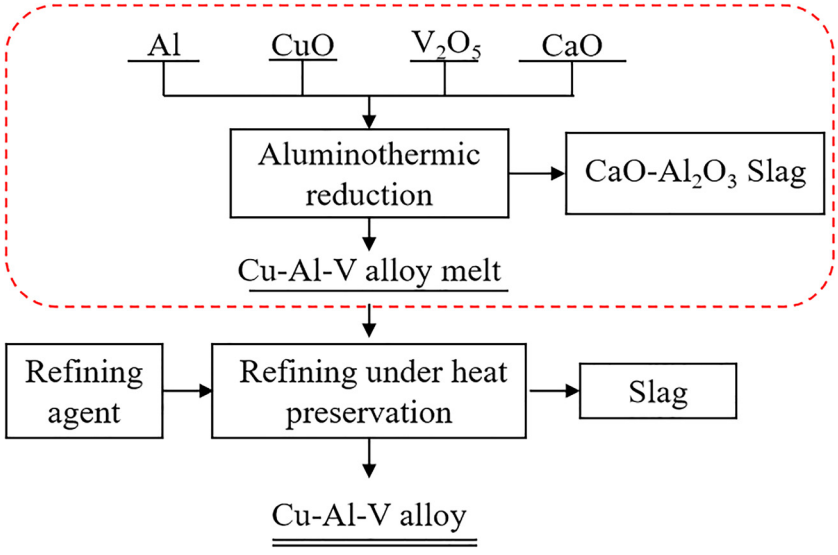

Figure 1: Short process of Cu–Al–V alloy preparation based on aluminothermic method.

3 Results and discussion

Based on the principle of thermodynamic equilibrium, the phase equilibrium relationship of Cu–Al–V system at 273 K was simulated by Factsage 6.4 software. The equilibrium phase diagram of Cu–Al–V ternary system is shown in Figure 2. The marked points A, B, and C in the Figure are the projection positions of the theoretical alloy composition calculated by HSC6.0 software in the phase diagram. The corresponding experimental groups a, b, and c are determined by the content of Cu–Al–V elements in the alloy measured by XRF, and the mass fraction of vanadium is distributed in the range of 5–20%. Thermodynamic analysis shows that when the system is in equilibrium, the composition points are located in region I of the phase diagram, but the experimental data show that all the measured points are concentrated in region II. The content of aluminum in the alloy is significantly higher than that of the calculated aluminum content. On the one hand, it is because Al exists in the alloy in the form of inclusions such as intermediate phase Al_xV_y (s) and alumina. On the other hand, the Gibbs free energy data of the Al_xV_y (s) phase are not included in the HSC6.0 thermodynamic database, which leads to the influence of the formation of the phase on the aluminum element in the theoretical calculation, resulting in the deviation of the calculated aluminum content from the measured value.

According to the proportion of components, the equilibrium point of the experiment is in region II. The results show that the combustion product is solid, and it is difficult to separate the alloy from the slag phase [31]. Therefore, calcium oxide is added to the system to produce $(CaO)_x(Al_2O_3)_y$ with low viscosity and low melting point, which accelerates the separation of the alloy from the slag [32,33]. In this study, the aluminothermic reduction method is used to control the content of vanadium, so that vanadium pentoxide reacts with aluminum to form metal vanadium and nano-intermediate phase Al_xV_y (s) [34].

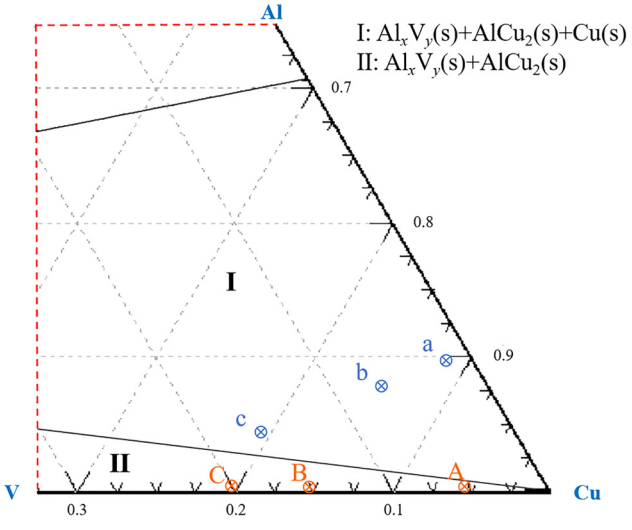

Figure 2: Equilibrium diagram of the Cu–Al–V system at 273 K.

3.1 Thermodynamics

Based on the principle of minimal Gibbs free energy change, in this study, the thermodynamic equilibrium of the CuO–Al–V_2O_5–CaO system was calculated, by the equilibrium compositions module of HSC Chemistry 6.0. And the results are shown in Figure 3. The thermodynamic equilibrium diagrams of a, b, and c are 5, 15, and 20% of the V_2O_5 ratio, respectively.

Figure 3 shows that the alloy phase of the system is mainly composed of Cu and V, and the slag phase is mainly $CaO{\cdot}2Al_2O_3$, $CaO{\cdot}Al_2O_3$, Al_2O_3, and CaO, accompanied by a small amount of $CaO{\cdot}6Al_2O_3$. By comparing the three thermodynamic equilibrium diagrams of the vanadium content of 5% (a), 15% (b), and 20% (c), it can be concluded that the phase content of Al_2O_3, $CaO{\cdot}2Al_2O_3$, and $CaO{\cdot}Al_2O_3$ remained relatively stable in the temperature range of 273–2,300 K. When the temperature rises to the range of 2,300–3,650 K, the content of $CaO{\cdot}2Al_2O_3$ and $CaO{\cdot}Al_2O_3$ decreases with the increase in temperature, while the content of CaO and Al_2O_3 shows an upward trend. This shows that in this temperature range, the increase in temperature is not conducive to the formation of low melting point calcium aluminate slag phases such as $CaO{\cdot}Al_2O_3$ and $CaO{\cdot}2Al_2O_3$, but it will promote the side reactions of Cu_2O and $CuO{\cdot}Al_2O_3$.

Compared with a, b, c in Figure 3, it can be found that the V content and Al_2O_3 slag content in the alloy phase increase with the increase in V_2O_5 addition, which confirms that the reduction reaction of V_2O_5 is strengthened. The contents of $CaO{\cdot}2Al_2O_3$ and $CaO{\cdot}Al_2O_3$ in the slag phase increase significantly with the increase in V_2O_5 content, indicating that the introduction of V_2O_5 is beneficial to promote the formation of low melting point calcium aluminate. This phase composition change is beneficial to increase the density difference between the metal phase and the slag phase, thereby improving the metal and slag separation effect. Comparing the variation trend of Al content in Fig $3a_1$, b_1, and c_1, it is found that there is a deviation between the actual Al content calculation result and the theoretical prediction. It is found that this phenomenon is due to the fact that the HSC6.0 thermodynamic database does not contain the V_xAl_y intermetallic phase, resulting in a deviation in the distribution calculation of aluminum in the alloy phase.

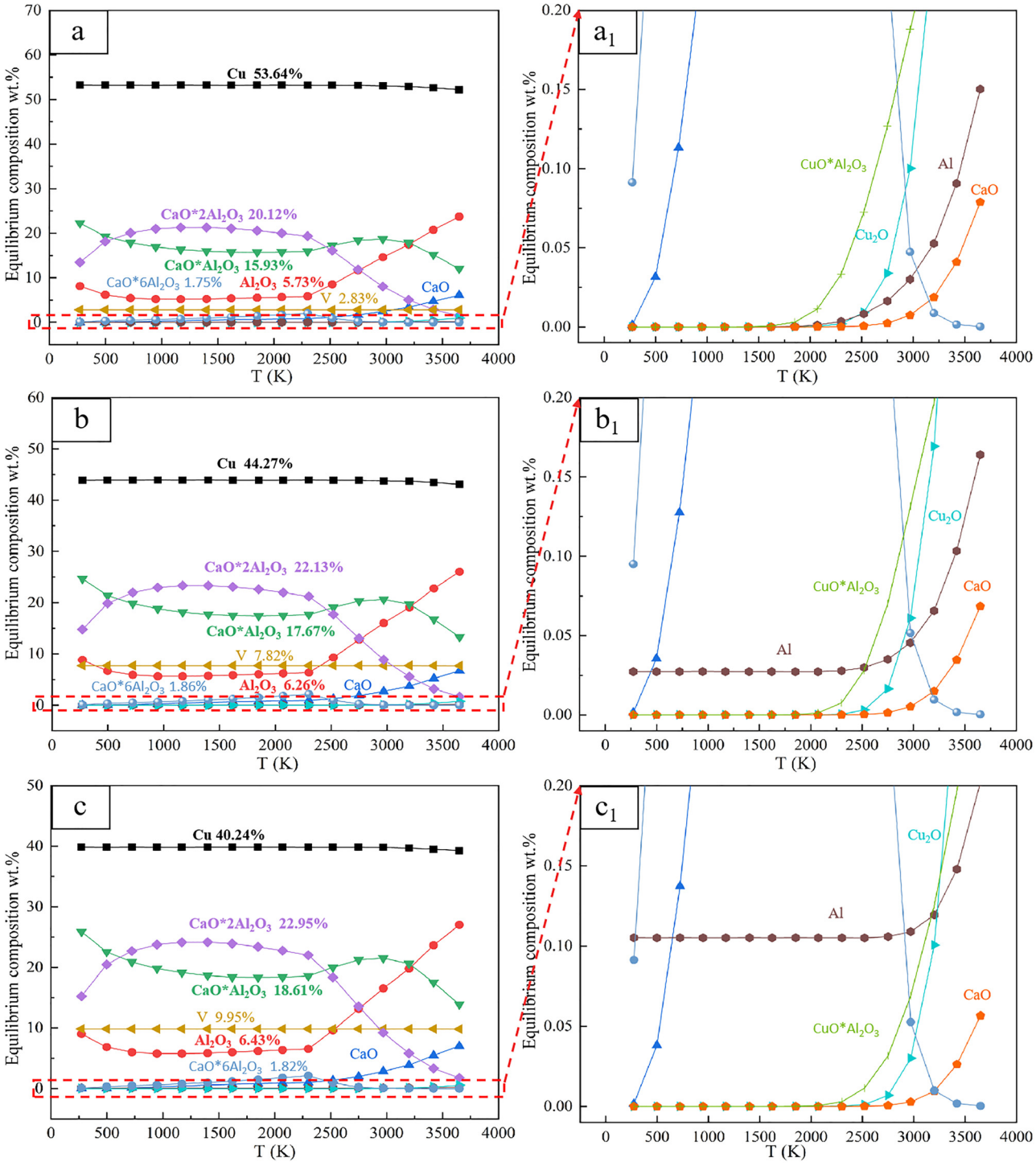

Figure 3: Thermodynamic equilibrium in CuO–Al–V_2O_5–CaO system. a, b and c are the thermodynamic equilibrium diagrams of the target vanadium content of 5, 15 and 20%, respectively. a_1, b_2 and c_3 are the local enlarged diagrams of a, b and c, respectively.

3.2 Characterization of Cu–Al–V alloys

3.2.1 Metallographic structure analysis

Figure 4 shows the microstructure evolution of Cu–Al–V alloys with different target vanadium contents (5, 15, 20%).

In Figure 4a, the vanadium particles are obviously agglomerated, the size distribution is uneven, and there are many incompletely separated slag phase inclusions in the matrix. In Figure 4b, the agglomeration of vanadium particles is reduced, the uniformity of dispersion distribution is significantly improved, and the number of slag

inclusions is reduced. In Figure 4c, the vanadium particles show a typical dendritic morphology and are evenly distributed along the matrix. The slag phase inclusions are very few and the dispersion is the lowest. Combined with the distribution characteristics of vanadium particles and the effect of slag phase separation, it can be concluded that with the increase in V_2O_5 ratio, the distribution uniformity of vanadium particles is gradually improved, and the number of slag inclusions is decreasing. This phenomenon is consistent with the thermodynamic calculation results (Figure 3) in which the increase in V_2O_5 content promotes the formation of low melting point calcium aluminate slag phase.

3.2.2 Microstructure analysis

Figure 5 is the scanning electron microscope (SEM) image of different vanadium contents.

From the a, b, c diagrams and element distribution diagrams, it can be seen that the alloy is mainly gray copper matrix, unevenly distributed with gray-white particles and black inclusions. Vanadium element is mainly distributed on gray-white particles, and a very small number is distributed on copper matrix. The aluminum and oxygen elements are mainly distributed on the black inclusions.

When the target vanadium content is 5%, the gray-white vanadium particles are approximately spherical, but there is local agglomeration. The average size is 4.15 μm, and the particle size range is between 0 and 10 μm. When the target vanadium content is 15%, the vanadium particles are snowflake-like and evenly distributed, with an average size of 8.72 μm and a particle size range of 0–25 μm. When the target vanadium content is 20%, the vanadium particles are further coarsened and present a dendritic distribution, and the distribution is more uniform. The average size is 7.06 μm, and the particle size range is between 0 and 35 μm.

In order to further analyze the copper matrix, the copper matrix was further enlarged, and it was found that white nanoparticles were distributed on the copper matrix. When the target vanadium content is 5%, the dispersed nanoparticles on the copper matrix are cubic, with an average size of 119.77 nm and a particle size distribution range of 0–600 nm. When the target vanadium content is 15%, the morphology of the nanoparticles on the copper matrix is transformed into a sphere, the average size is reduced to 79.23 nm, and the particle size distribution is

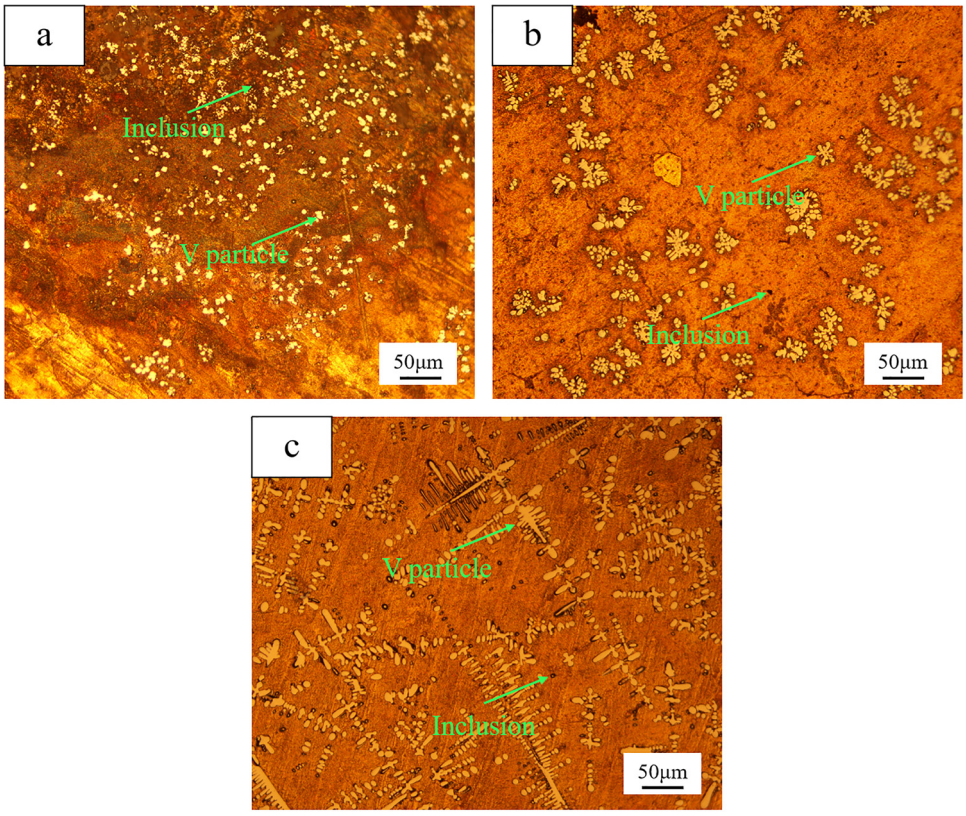

Figure 4: Cu–Al–V alloy metallographic diagram. a, b and c are the metallographic diagram of the target vanadium content of 5, 15 and 20%, respectively.

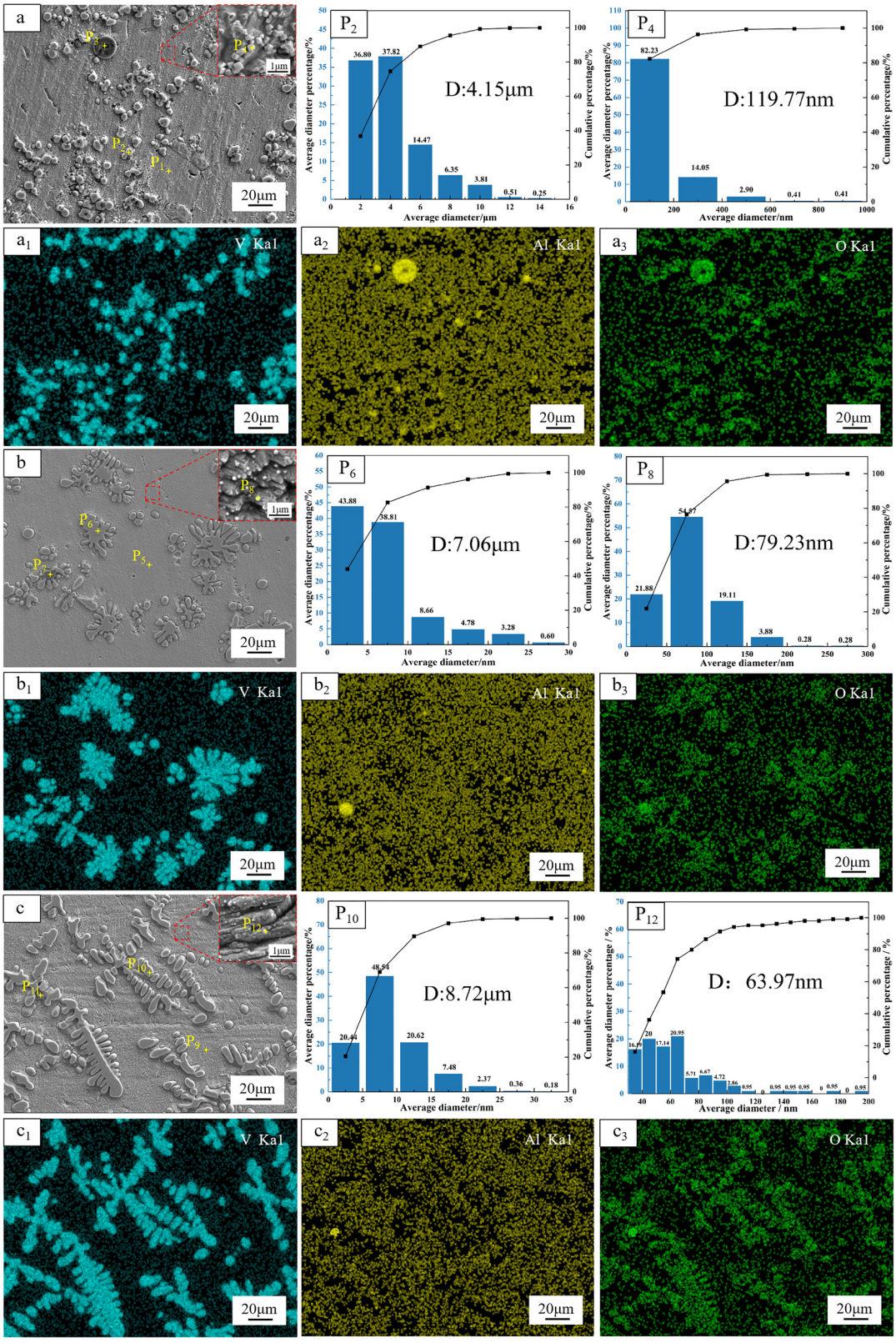

Figure 5: SEM images, particle size analysis and phase analysis of Cu-Al-V alloys with target. a, b, c represent the gold SEM images of the target vanadium contents of 5, 15, and 20% respectively, vanadium content of 5, 15 and 20%, a_1–a_3, b_1–b_3 and c_1–c_3 are element distribution, P_2, P_6, P_{10} are V particle size analysis, P_4, P_8, P_{12} vanadium–aluminum intermediate alloy phase particle size distribution.

narrowed to 0–200 nm. When the target vanadium content is 20%, the nanoparticle phase is still spherical, but the average size is further reduced to 63.97 nm, and the particle size distribution is concentrated at 0–120 nm. The analysis of black inclusions on copper matrix shows that when the target vanadium content is 5%, the size of black inclusions is large and obvious. As the V_2O_5 ratio increases, the inclusions gradually decrease and are distributed in the middle of the vanadium particles, which indicates that the inclusions in the middle of the vanadium particles are not easily separated from the copper melt. It can be seen that with the increase in V_2O_5 ratio in the alloy, the number of unseparated slag phases in the alloy decreases significantly, which is consistent with the thermodynamic calculation results (formation of low melting point calcium aluminate slag phase). It is confirmed that the increase in V_2O_5 ratio in the alloy is beneficial to improve the fluidity of slag phase, thus improving the separation efficiency of slag and metal.

In summary, the increase in V_2O_5 ratio promotes the uniform coarsening and dendrite growth of vanadium particles by regulating the aluminothermic reduction kinetic process, while inhibiting the coarsening of nanophase and enhancing its dispersion strengthening effect. This process is accompanied by a significant reduction in slag phase residues, indicating that the increase in V_2O_5 ratio can simultaneously optimize the microstructure of Cu–Al–V alloy and the separation efficiency of metal and slag, which provides an important basis for the design of high-performance copper matrix composites. Micron-sized vanadium particles were observed in all alloys with varying vanadium contents, which is consistent with the thermodynamic calculations predicting the precipitation of elemental vanadium, as shown in Figure 3.

Figure 6 reveals the element distribution characteristics and inclusion composition of Cu–Al–V alloys with different target vanadium contents (5, 15, and 20%) by energy dispersive spectroscopy (EDS) surface distribution and micro-point analysis.

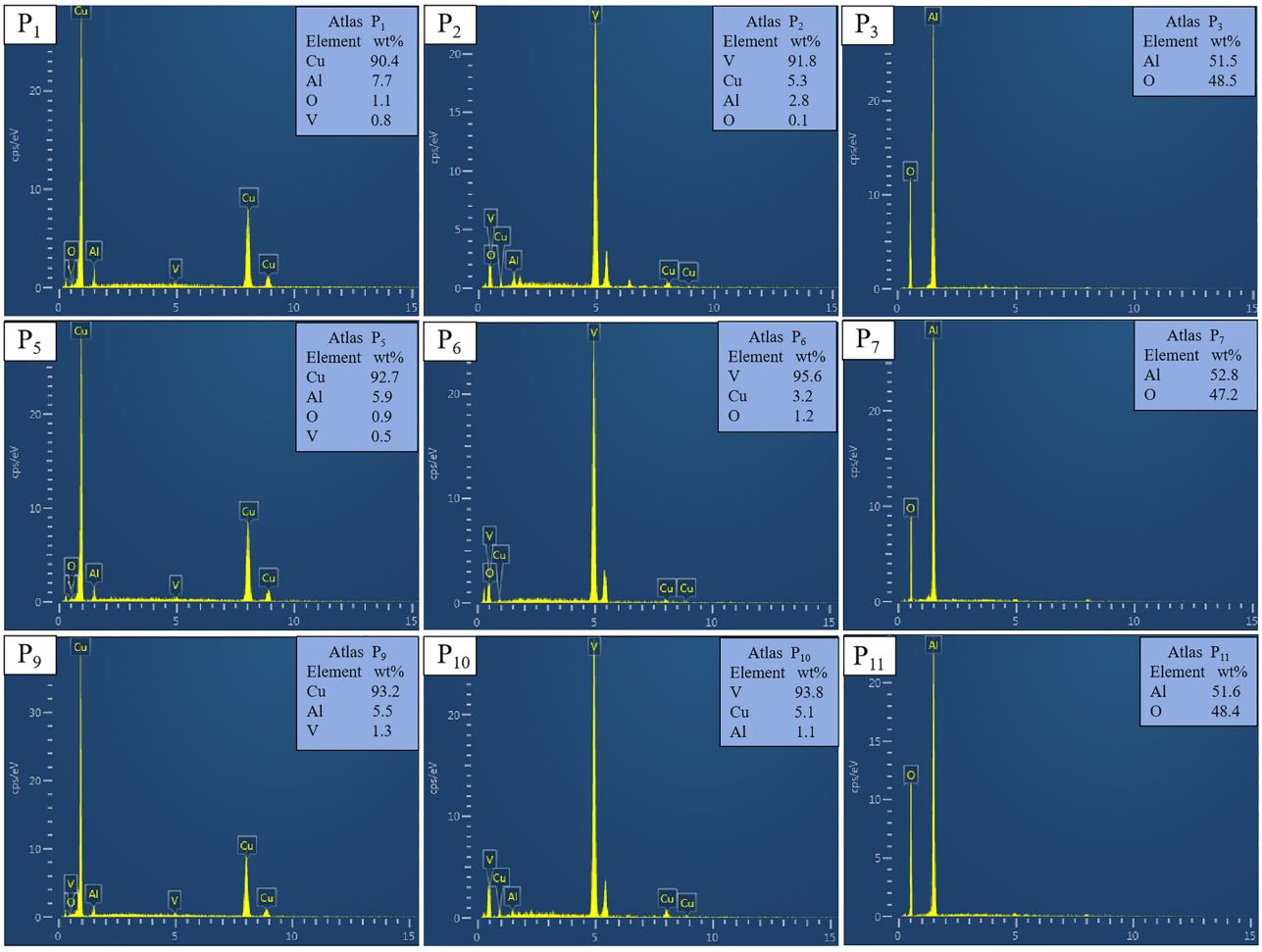

Figure 6: EDS analysis diagram of Cu–Al–V alloy; P_1, P_5, and P_9 are EDS analysis of alloy matrix, P_2, P_6, and P_{10} are EDS analysis of V particles, and P_3, P_7, and P_{11} are EDS analysis of inclusions.

Combined with the microstructure of Figure 5 and the quantitative composition data of Figure 6, it can be concluded that: Figure P_1, P_5, and P_9 are mainly copper elements, accompanied by a small amount of V and Al solid solution, indicating that the matrix is a solid solution phase dominated by Cu. P_2, P_6, and P_{10} are mainly vanadium elements, corresponding to the vanadium particle phase observed in Figure 5. P_3, P_7, and P_{11} are inclusion phase diagrams, in which P_3, P_7, P_{11} point to Al:O atomic ratios close to 2:3, consistent with the theoretical composition of Al_2O_3. In summary, EDS analysis confirmed that there was significant element differentiation among the matrix, particle phase, and inclusions of Cu–Al–V alloy.

In order to further explore the nanoparticle phase on the copper matrix, it was characterized and analyzed by TEM, as shown in Figure 7.

In Figure 7a, the matrix nanoparticles are sparsely distributed, and the phase is determined to be Al_3V by SAED spot calibration. The crystal band axis is [−9,−2,−1], tetragonal structure, and the space group is I4/mmm. The distribution of nanoparticles in Figure 7b still has local aggregation. SAED analysis shows that the crystal belt axis is [−4,−15,−6], which confirms that the phase is hexagonal $Al_{23}V_4$, and the space group is $P6_3/mmc$. The nanoparticles in Figure 7c are uniformly dispersed. SAED calibration shows that the phase is AlV_3, crystal zone axis [2,4,5], simple cubic structure, space group Pm-3m. The transformation from Al_3V to AlV_3 reflects the significant effect of the increase in vanadium activity on the stability of Al–V intermetallic compounds, which is consistent with the composition-temperature dependence of Al–V binary phase diagram [35,36]. TEM analysis reveals the composition-structure-size co-evolution of Al_xV_y nanophase in Cu–Al–V alloy. The increase in V_2O_5 ratio drives the transformation of nanophase from Al_3V to AlV_3 by adjusting the Al/V atomic. The calculated phase compositions of

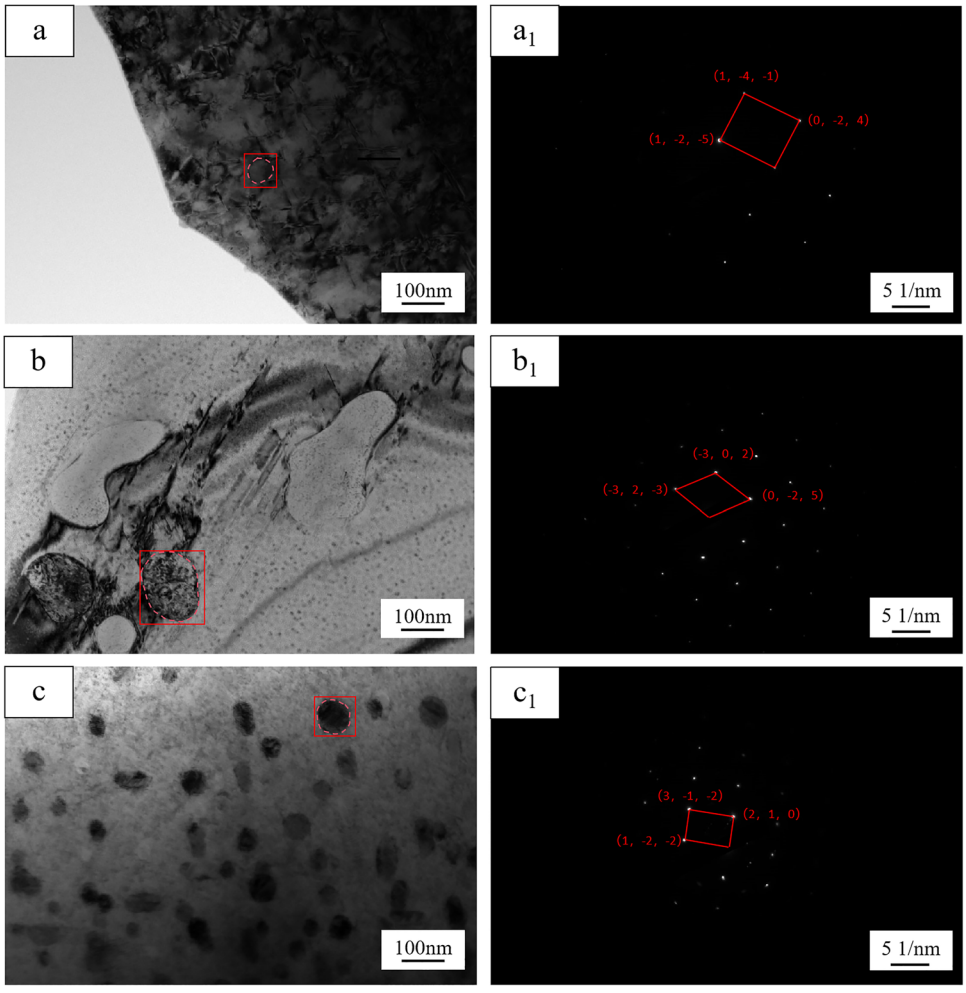

Figure 7: TEM images of nanoparticles in Cu–Al–V alloy: a, b, and c are nanoparticle images with vanadium content of 5, 15, and 20%, respectively; a_1, b_1, and c_1 are the diffraction patterns of the marked regions in a, b, and c.

vanadium metal and Al_xV_y intermetallic compounds (Figures 2 and 3) exhibit striking consistency with the experimentally determined phase analysis results of the alloy (Figures 5–7). This close agreement robustly validates the feasibility of synthesizing dual-phase micro-nano alloys *via* metallothermic reduction.

In order to further study the variation in inclusions in the alloy, the bulk alloy was dissolved with $FeCl_3$ solution to obtain inclusions in the alloy, as shown in Figure 8.

When the content of V is 5%, the inclusions are mainly spherical, accounting for 58.90%, accompanied by some irregular particles. The EDS spectrum shows that the atomic ratios of Al and O of spherical and irregular particles are 2.03:2.82 and 1.98:2.90, respectively, which are highly consistent with the theoretical value of Al_2O_3 (2:3). It is confirmed that both spherical and irregular particles are alumina phase, and the average particle size is 65.96 μm. When the V content is 15%, the proportion of spherical inclusions decreases to 51.78%, and the irregular alumina phase increases. The atomic ratio of Al and O is maintained at 2:3, and the phase is still Al_2O_3, and the average particle size is reduced to 42.20 μm. When the V content is 20%, the spherical inclusions are at least 32.24%. EDS analysis shows that the atomic ratio of Al to O is close to 2:3. It is inferred that the inclusions are alumina, and the average particle size is 53.7 2μm.

As the V_2O_5 ratio gradually increases, the spherical alumina in the alloy gradually decreases, which may be due to the increase in V_2O_5 ratio inhibiting the transformation of irregular alumina (γ-Al_2O_3) to spherical alumina (α-Al_2O_3). The adiabatic temperatures of different V_2O_5 ratio are calculated using formula (1). The adiabatic temperatures of 5, 15, and 20% vanadium contents are 2569.15, 2489.15, and 2413.15 K, respectively.

$$Q = \Delta H^{\theta}_{298.15\mathrm{K}} + \int_{298.15\mathrm{K}}^{T\mathrm{ad}} \sum (vicpi)\mathrm{d}T. \quad (1)$$

Therefore, with the increase in the V_2O_5 ratio, the adiabatic temperature of the system decreases, which is not conducive to the transformation of metastable γ-Al_2O_3 to stable α-Al_2O_3, resulting in the decrease in spherical alumina in the alloy [37–39].

3.3 Characterizations of the slag

Figure 9 is the phase composition of the slag after aluminothermic reduction.

The characteristic diffraction peaks of $CaAl_4O_7$ and Cu_2O were clearly detected in diagram (a), indicating that calcium aluminate and cuprous oxide are the main stable phases of the slag system under this condition, which was consistent with the thermodynamic trend of Al preferential reduction of Cu_2O in the aluminothermic reduction

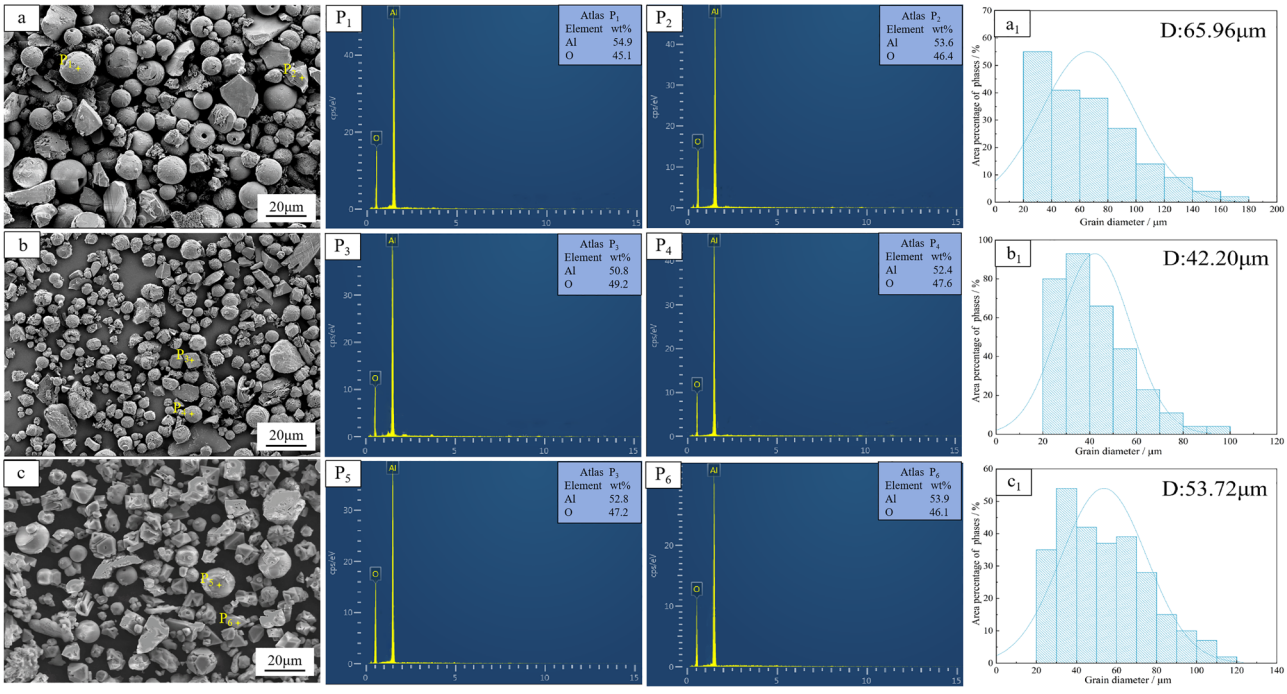

Figure 8: SEM images of inclusions in Cu–Al–V alloy: (a, b, and c) SEM images of inclusions in the V content of 5, 15, and 20%, respectively. (P_1–P_6) EDS maps of the marker points in a, b, and c. (a_1, b_1, and c_1) Particle size analysis of a, b, and c.

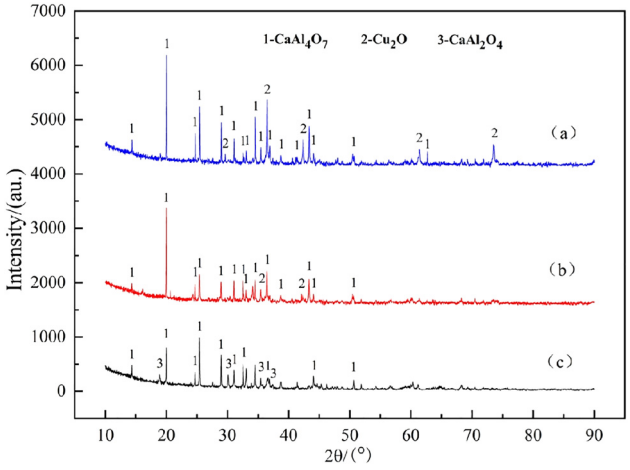

Figure 9: XRD pattern of Cu–Al–V slag phase with V_2O_5 ratio of 5% (a), 15% (b), and 20% (c).

reaction. In Figure (b), $CaAl_4O_7$ and Cu_2O are still the main phases, and the intensity of Cu_2O peak is significantly weakened, which reflects that the increase in V_2O_5 ratio enhances the reduction efficiency of reducing agent to Cu_2O, resulting in the decrease in residual amount. The diffraction peaks of $CaAl_4O_7$ and $CaAl_2O_4$ appear in Figure (c), and the diffraction peak of Cu_2O is basically not detected, indicating that the reduction reaction tends to be complete when the V_2O_5 ratio reaches 20%, and the copper oxide is completely reduced to the metal phase. The transformation of $CaAl_4O_7$ to $CaAl_2O_4$ may be related to the increase in the ratio of CaO/Al_2O_3. When the ratio of CaO/Al_2O_3 increases, the viscosity of the slag decreases [40–42].

Table 1 is the composition of reducing slag with V_2O_5 ratio of 5% (1#), 15% (2#), and 20% (3#), respectively. It can be seen from Table 1 that the reducing slag composition includes Al_2O_3, CuO, CaO, V_2O_5, *etc.* With the increase in V_2O_5 content in the material, the contents of Al_2O_3, CaO, and V_2O_5 in the slag gradually increased, and the content of CuO gradually decreased. The results show that the main phase of the reduced slag in 1# and 2# is calcium aluminate $CaAl_4O_7$, and its layered structure leads to higher viscosity of the slag. With the increase in V_2O_5 content, $CaAl_4O_7$ transforms to $CaAl_2O_4$, and the cubic spinel structure reduces the melt viscosity. At the same time, the formation of $CaAl_2O_4$ phase reduces the melting point of slag system to 1,350–1,400°C, and the interfacial tension between slag and gold decreases, which significantly improves the separation efficiency of metal and slag. The increase in V content promotes the reduction of CuO.

Table 1: Composition of reducing slag (wt%)

Component	Al_2O_3	CuO	CaO	V_2O_5	Others
1#	53.81	20.38	16.73	3.94	5.14
2#	59.79	5.78	18.62	13.33	2.48
3#	62.57	1.28	20.86	13.61	1.68

4 Conclusion

1) The Cu–Al–V alloy melts reinforced by micro-nano particles was successfully prepared by aluminothermic reduction method. The micron-sized vanadium particles synthesized *in situ* in the alloy range from 1 to 10 μm, and the nano-sized Al_3V, $Al_{23}V_4$, AlV_3 particles range from 60 to 200 nm.
2) The microstructure of Cu–Al–V alloy melts prepared by aluminothermic reduction is mainly composed of nano-sized Al_3V, $Al_{23}V_4$, AlV_3 particles dispersed in copper matrix, micron-sized vanadium particles and spherical, irregularly shaped alumina inclusions. With the increase in V_2O_5 ratio, the particle size of vanadium increases and the particle size of nano vanadium aluminum intermediate alloy decreases gradually. The inclusions are composed of spherical and irregular alumina, and the proportion of spherical alumina gradually decreases from 58.90 to 32.24%.
3) The slag obtained after reduction is mainly composed of $CaAl_4O_7$, $CaAl_2O_4$, and Cu_2O. With the increase in V_2O_5 ratio, the high melting point $CaAl_4O_7$ in the slag decreases and the low melting point $CaAl_2O_4$ increases, which is beneficial to the separation of slag and metal.

Acknowledgments: The authors are especially thankful to the Zhongyuan Youth Talent Support Program (No. Chu Cheng [2024]), the Henan Province Natural Science Foundation Project (No. 252300420026), the Key Technologies R&D Program of Henan Province (No. 242102231024), the Youth Talent Support Program of He Luo (No. 2024HLTJ18), the Key Technologies R&D Program of Sanmenxia City (No. 2023L02012), the Foundation for Key Teacher by Henan University of Science and Technology (No. 13450026).

Funding information: The Zhongyuan Youth Talent Support Program (No. Chu Cheng [2024]), the Henan Province Natural Science Foundation Project (No. 252300420026), the Key Technologies R&D Program of Henan Province (No. 242102231024), the Youth Talent Support Program of He Luo (No. 2024HLTJ18), the Key Technologies R&D Program of Sanmenxia City (No. 2023L02012), the Foundation for Key

Teacher by Henan University of Science and Technology (No. 13450026).

Author contributions: All authors have accepted responsibility for the entire content of this manuscript and approved its submission.

Conflict of interest: The authors state no conflict of interest.

Data availability statement: All data generated or analyzed during this study are included in this published article.

References

[1] Wu Q, Xu Z, Huang W, Qi X, Wu J, Du J, et al. Enhanced strength of a high-conductivity Cu-Cr alloy by Sc addition. Rare Met. 2024;43(11):6054–67.

[2] Yi X, Ma A, Zheng Y, Li Y, Li J, Zhao M, et al. Elucidating different selective corrosion behavior of two typical marine aluminum bronze alloys from the perspective of constituent phases. Corros Sci. 2024;235:235112167.

[3] Wang YD, Liu M, Yu BH, Wu LH, Xue P, Ni DR, et al. Enhanced combination of mechanical properties and electrical conductivity of a hard state Cu-Cr-Zr alloy *via* one-step friction stir processing. J Mater Process Technol. 2021;288:116880.

[4] Zhang XD, Jiang YH, Cao F, Yang T, Gao F, Liang SH. Hybrid effect on mechanical properties and high-temperature performance of copper matrix composite reinforced with micro-nano dual-scale particles. J Mater Sci Technol. 2024;172:94–103.

[5] Li Z, Jiang X, Sun H, Liu S, Pang Y, Wu Z, et al. Microstructure and mechanical properties of Cu\Ni-coated α-Al_2O_{3w} and graphene nano-platelets co-reinforced copper matrix composites. Mater Chem Phys. 2024;325:129772.

[6] Qian L, Zhang J, Yang W, Wang Y, Chan K, Yang XS. Maintaining grain boundary segregation-induced strengthening effect in extremely fine nanograined metals. Nano Lett. 2025;25(13):5493–501.

[7] Zhou CL, Chen ZN, Guo EY, Kang HJ, Fan JH, Wang W, et al. A nano-micro dual-scale particulate-reinforced copper matrix composite with high strength, high electrical conductivity and superior wear resistance. RSC Adv. 2018;8(54):30777–82.

[8] Zhu JL, Zhong LS, Xu YH, Li JL, Zhang SX, Lu ZX. Fabrication of a novel multi-sized and layered (Ti_x,Nb_{1-x})C surface-reinforced layer on TiNb alloy. Mater Res Express. 2019;6(10):106512.

[9] Lv L, Jiang X, Xiao X, Sun H, Shao Z, Luo Z. Study on corrosion resistance of copper matrix composites reinforced by Al_2O_3 whiskers. Mater Res Express. 2020;7(2):026534.

[10] Thankachan T, Prakash SK, Kavimani V. Effect of friction stir processing and hybrid reinforcements on copper. Mater Manuf Process. 2018;33(15):1681–92.

[11] Chen WP, Li ZX, Lu TW, He TB, Li RK, Li B, et al. Effect of ball milling on microstructure and mechanical properties of 6061Al matrix composites reinforced with high-entropy alloy particles. Mater Sci Eng A. 2019;762:138116.

[12] Zhu R, Sun Y, Feng J, Gong W, Li Y. Effect of microstructure on mechanical properties of FeCoNiCrAl high entropy alloys particle reinforced Cu matrix surface composite prepared by FSP. J Mater Res Technol. 2023;27:2695–708.

[13] Wang YH, Zang JB, Wang MZ, Guan Y, Zheng YZ. Properties and applications of Ti-coated diamond grits. J Mater Process Technol. 2002;129(1):369–72.

[14] Ciupiński Ł, Siemiaszko D, Rosiński M, Michalski A, Kurzydlowski KJ. Heat sink materials processing by pulse plasma sintering. Adv Mater Res. 2008;59:120–4.

[15] Wang XZ, Su YH, Ouyang QB, Zhu CN, Cao H, Zhang D. Fabrication, mechanical and thermal properties of copper coated graphite films reinforced copper matrix laminated composites *via* ultrasonic-assisted electroless plating and vacuum hot-pressing sintering. Mater Sci Eng A. 2021;824:144768.

[16] Yang Q, Duan J, Deng A, Wang E. Numerical simulation of macrosegregation phenomenon in Cu-6wt%Ag alloy ingots fabricated by electromagnetic stirring. J Mater Res Technol. 2024;28:300–15.

[17] Liu C, Yin Y, Li C, Xu M, Li R, Chen Q. Tailoring Cu nano Bi self-lubricating alloy material by shift-speed ball milling flake powder metallurgy. J Alloy Compd. 2022;903:163747.

[18] Jisen Y, Minghui W, Tingan Z, Fang X, Xi Z, Ke Z, et al. Research progress in preparation technology of micro and nano titanium alloy powder. Nanotechnol Rev. 2024;13(1):20240016.

[19] Pan Y, Lu X, Volinsky AA, Liu B, Xiao S, Zhou C, et al. Tribological and mechanical properties of copper matrix composites reinforced with carbon nanotube and alumina nanoparticles. Mater Res Express. 2019;6(11):116524.

[20] Shen DP, Zhu YJ, Yang X, Tong WP. Investigation on the microstructure and properties of Cu-Cr alloy prepared by in-situ synthesis method. Vacuum. 2018;149:207–13.

[21] Zhang SR, Kang HJ, Li RG, Zou CL, Guo EY, Chen ZE, et al. Microstructure evolution electrical conductivity and mechanical properties of dual-scale Cu_5Zr/ZrB_2 particulate reinforced copper matrix composites. Mater Sci Eng A. 2019;762:138108.

[22] Li N, Zhang F, Yang Q, Wu Y, Wang M, Liu J, et al. Microstructure and mechanical properties of in situ TiB_2/2024 composites fabricated by powder metallurgy. J Mater Eng Perform. 2022;31(11):8775–83.

[23] Zhang DY, Yang F, Zhao HX, Ding ZJ, Wan JP, Ren YC, et al. Microstructure, mechanical property and wear resistance of in-situ TiC/Ti64 composites *via* adding graphite in irregular Ti64 powder. Materials Today. Communications. 2025;42:111381.

[24] Song YL, Dou ZH, Zhang TA, Liu Y. Research progress on the extractive metallurgy of titanium alloys. Min Process Extr Metall Rev. 2020;3:1–16.

[25] An W, Dou ZH, Zhang TA. Microstructure uniformity control of CuCr alloy prepared in-situ by aluminothermic reduction coupled with permanent magnetic stirring. J Alloy Compd. 2023;96:170797.

[26] Song Y, Dou Z, Liu Y, Zhang T. Study on the preparation process of TiAl alloy by self-propagating metallurgy. J Mater Eng Perform. 2024;33(2):660–9.

[27] An W, Dou ZH, Han JR, Zhang TA. Microstructure evolution and property strengthening of CuCr50 prepared by thermite reduction-electromagnetic casting during the heat treatment process. J Mater Res Technol. 2023;24:6533–44.

[28] Wang XY, Cheng C, Feng YS, Wang MX, Li MY, Huang T, et al. Microstructure regulation mechanism of CuW composites

prepared by aluminothermic coupling with magnesiothermic reduction. J Mater Res Technol. 2025;34:2684–97.
[29] Fan SG, Dou ZH, Zhang TA, Yan JS. Self-propagating reaction mechanism of $MgTiO_2$ system in preparation process of titanium powder by multi-stage reduction. Rare Met. 2020;40(9):1–12.
[30] Nersisyan HH, Lee JH, Won CW. A study of tungsten nanopowder formation by self-propagating high-temperature synthesis. Combust Flame. 2005;142:241–8.
[31] Cheng C, Dou ZH, Zhang TA, Zhang HJ, Yi X, Su JM. Synthesis of as-cast Ti–Al–V alloy from titanium-rich material by thermite reduction. JOM. 2017;69(10):1818–23.
[32] Wang P, Gong W, Jiang Z, Li X, Zhang Y. Effect of MgO content and CaO/Al_2O_3 ratio on melting temperature and viscosity of CaF_2-CaO-Al_2O_3-MgO slag for electroslag remelting. Ceram Int. 2024;50(19PB):36829–37.
[33] Song M, Liu J. Novel insight into the preparation of Ti-6Al-4V alloy through thermite reduction based on the mass action concentration. J Wuhan Univ Technol-Mater Sci Ed. 2023;38(3):652–8.
[34] Song Y, Dou Z, Zhang T, Cheng C, Fang H, Ban CL. Thermodynamic insight into the equilibrium component prediction in the Al-Ti-Ca-oxide system. Arch Metall Mater. 2023;68(4):1319–26.
[35] Okamoto H. Al–V (Aluminum–Vanadium). J Phase Equilibria Diffus. 2012;33(6):491.
[36] Shi ZB, Ma CF, Wang F, Liu P, Liu XK, Li W. Calculation assessment and activity of the Al–V binary phase diagram. Nonferrous Met Mater Eng. 2017;38(04):222–8.
[37] Kang S, Zhao X, Guo J, Liang J, Sun J, Yang Y, et al. Thermal-assisted cold sintering study of Al_2O_3 ceramics: Enabled with a soluble γ-Al_2O_3 intermediate phase. J Eur Ceram Soc. 2023;43(2):478–85.
[38] Dynys FW, Halloran JW. Alpha alumina formation in alum-derived gamma alumina. J Am Ceram Soc. 2010;65(9):442–8.
[39] Ali AMMA, Amin SAA, Adnan A. Effect of copper oxide (CuO) and vanadium oxide (V_2O_5) addition on the structural, optical and electrical properties of corundum (α-Al_2O_3). Sci Rep. 2023;13(1):16100.
[40] Wen Y, Shu Q, Lin Y, Fabritius T. Effect of SiO_2 content and mass ratio of CaO to Al_2O_3 on the Viscosity and Structure of CaO-Al_2O_3-B_2O_3-SiO_2 Slags. ISIJ Int. 2023;63:1–9.
[41] Song Y, Dou Z, Zhang T, Wang G. Mechanisms of metal-slag separation behavior in thermite reduction for preparation of TiAl Alloy. J Mater Eng Perform. 2021;30(12):1–11.
[42] Cheng C, Wang XY, Song KX, Song ZW, Dou ZH, Zhang Me, et al. Effects of CaO addition on the CuW composite containing micro- and nano-sized tungsten particles synthesized *via* aluminothermic coupling with silicothermic reduction. Nanotechnol Rev. 2023;12(1):20220507.